Effect of normal load on the crack propagation from pre-existing joints using Particle Flow Code (PFC)

Hadi Haeri[1a], Vahab Sarfarazi[2*] and Zheming Zhu[3]

[1]*Young Researchers and Elite Club, Bafgh Branch, Islamic Azad University, Bafgh, Iran*
[2]*Department of Mining Engineering, Hamedan University of Technology, Hamedan, Iran*
[3]*College of Architecture and Environment, Sichuan University, Chengdu 610065, China*

Abstract. In this paper, the effect of normal load on the failure mechanism of echelon joint has been studied using PFC2D. In the first step, calibration of PFC was undertaken with respect to the data obtained from experimental laboratory tests. Then, six different models consisting various echelon joint were prepared and tested under two low and high normal loads. Furthermore, validation of the simulated models were cross checked with the results of direct shear tests performed on non-persistent jointed physical models. The simulations demonstrated that failure patterns were mostly influenced by normal loading, while the shear strength was linked to failure mechanism. When ligament angle is less than 90°, the stable crack growth length is increased by increasing the normal loading. In this condition, fish eyes failure pattern occur in rock bridge. With higher ligament angles, the rock bridge was broken under high normal loading. Applying higher normal loading increases the number of fracture sets while dilation angle and mean orientations of fracture sets with respect to ligament direction will be decreased.

Keywords: particle flow code; rock bridge angle; normal load; shear and tensile cracks

1. Introduction

There are only few cases where the location of a rock structure failure is limited to a single discontinuity. Usually several discontinuities of limited sizes interact and eventually form a combined shear plane. Besides adjacent discontinuities themselves, regions between them consisted of a strong rock, named the rock bridges (Fig. 1) of utmost importance for the shear strength of compound failure plane (Jaeger 1973, Olson and Pollard 1991).

A lack of understanding exists regarding processes and types of breakages and the failure of a discontinuous shear plane consisting weak and separated as well as intact sections (Haeri 2015a). Failure process for such discontinuous joints has been investigated only to a limited extent. Previous experiments based on uniaxial or biaxial tests on specimens with inserted, mostly parallel cracks and the rock bridges between them were concentrated on crack growth and crack coalescence (Zhao 1995, Bobet 1998, Sagong 2002, Mughieda and Khawaldeh 2004, Mughieda and Alzoubi 2004, Fujii and Ishijima 2004, Li *et al.* 2005, Mughieda and Khawaldeh 2006, Yang *et al.* 2008, 2009, Haeri 2011, Haeri and Ahranjani 2012, Kumar and Barai 2012, Zhang and Wong 2012, 2013, Haeri *et al.* 2013a, b, Wasantha *et al.* 2014b, Xie *et al.* 2014, Jiang *et al.* 2014, Haeri *et al.* 2014a, 2014b, Haeri *et al.* 2015a, Haeri *et al.* 2015b, Haeri *et al.* 2015c, Haeri 2015d, 2015e, 2015f, Haeri

et al. 2016).

Direct shear testing on regularly stepped joints can be employed for better understanding of shear strength of formerly discontinuous joints. Gehle and Kutter's (2003), investigation on the breakage and shear behaviour of intermittent rock joints under direct shear loading showed that, the joint orientation is an important and influential parameter for shear resistance of jointed rocks. Ghazvinian *et al.* (2007), made a thorough analysis in shear behaviour of rock-bridges based on the changes in their areas persistency**.** Analysis showed that, the failure mode and mechanism are affected by the rock-bridge continuity. Haeri *et al.* (2016) has investigated the shear behaviour of planar non-persistent joint. He found that the shear failure mode in bridge changes to the tensile failure mode by increasing in the effective joint Coefficient. Sarfarazi *et al.* (2016) has investigated the effect of non-persistent joints on sliding direction of rock slope. He found that the shear strength is closely related to the rock bridge failure pattern and failure mechanism, so that in the fixed area of the rock-bridge under fixed normal stress, the rock-bridge resistance reduced with change in failure mode from shear to tensile.

In recent years, numerical modeling techniques for fracturing process simulation have been widely used in rock engineering. A large number of numerical methods such as finite element method, boundary element method, discrete element method and displacement discontinuity method, have been used to study the fracture of rock bridge. The random particle model presented by Bazant *et al.* (1990), UDEC used by Vonk *et al.* (1991), mechanical model proposed by Mohamed and Hansen (1999), PFC2D used by Sarfarazi *et al.* (2014), Bahaaddini *et al.* (2013), are all of typical numerical models for simulating the materials

---

∗Corresponding author, Assistant Professor
 E-mail: vahab.sarfarazi@gmail.com
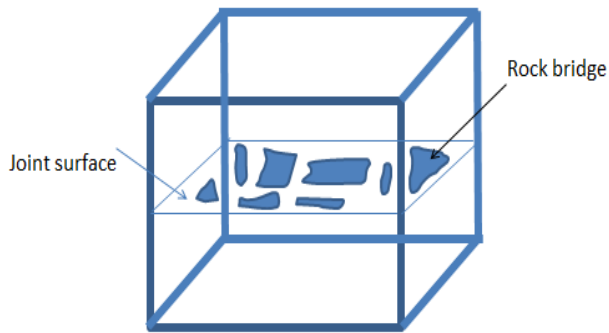[a]Assistant Professor

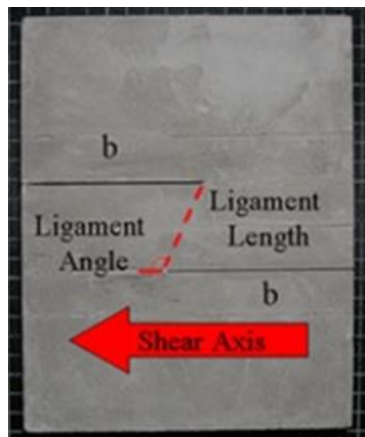Fig. 1 Distribution of rock bridge and rock joint in shear surface

Fig. 2 Schematic view of ligament length and ligament angle in a non-persistent joint

fracturing mechanisms.

In previous work the effect of normal load was eliminated on the shear behaviour of rock bridge.

In this paper, a particle flow code was used to study the shear failure behaviour of en-echelon joints under low and high normal loadings. The effect of normal load on the crack initiation stress and failure stress were determined. Also, the ability of PFC2D in determining failure patterns in rock bridges was checked by comparing the numerical with experimental results.

For this purpose, an inverse modelling calibration approach and the laboratory results for uniaxial, Brazilian, and tri-axial tests were used to estimate the intact rock's micromechanical parameters used in our simulation. Validation of the simulation was then performed by the comparison between the shear behaviour of rock bridges in PFC2D and that of the en-echelon joints tested under direct shear loadings in the laboratory. Validated numerical model was used to further studying the mechanical behaviour of jointed models with different joint persistency.

2. Laboratory tests

2.1 Preparation and testing of the rock like model

The model material used in preparing the intact samples and jointed blocks was a mixture of plaster

Table 1 Properties of the intact model material determined experimentally, Ghazvinian *et al.* (2012)

Property	Value
Average uniaxial compressive strength (MPa)	6.6
Average Brazilian strength (MPa)	1
Average Young's modulus in compression (GPa)	5.4
Average Poisson's ratio	0.18
Internal friction angle	20.4
Cohesion (MPa)	2.2

(37.5%), cement (25%) and water (37.5%). Mixing, casting, curing of the specimens and their dimensions has been described in details by Ghazvinian *et al.* (2012).

Uniaxial/tri-axial compression and the Brazilian tensile tests were performed in Rock Mechanics Laboratory of Graz University of Technology by the Machine Tool System (MTS) in order to determine the mechanical properties of intact model material. Mechanical properties of the physical models are summarized in Table 1.

2.2 Preparation, testing and results of the rock like model consisting of en-echelon joints

Four specimens with similar ligament length of 45 mm and different ligament angles of 0°, 25°, 90°, and 115° were prepared (ligament length is the distance between the tips of two joints, and ligament angle is the counterclockwise angle between ligament length and shear axis; Fig. 2. The lengths of two edge joints are equal in each sample but they vary in different specimens. The joints lengths (b) are at 52.5, 66.8, 75, and 78.8 mm associated with the ligament angles of 0°, 25°, 90°, and 115°, respectively. Two similar samples were prepared from each specimen and tested in two different normal loadings; 0.3 MPa and 2.5 MPa which are at 5% and 38% of the uniaxial strength of intact material, respectively. The procedures of mixing, casting, curing and testing of jointed blocks were introduced in details by Sarfarazi *et al.* (2014).

A servo-controlled MTS direct shear apparatus with a modified shear box was used for testing artificial echelon joints. All samples were tested with a shear displacement rate of 0.01 mm/s. Fig. 3 shows the failure patterns obtained from direct shear tests. Observation results showed that the normal loads influence the failure pattern of the rock bridges.

When ligament angle is 0°, under low normal loading (Fig. 3(a)), the upper tensile crack propagates through the intact portion area. But, the lower tensile crack develops only for a short distance, and then becomes stable so as not to connecting with the tip of other joint. Failure surface of the bridge area is tensile because no crushed or pulverized materials existed and no evidence of shear movement was noticed along the failure surface. Mean orientation of failure surface related to ligament direction was nearly 43°. Dilation angle in this configuration was close to 36°.

Dilation angle is measured as the ratio of vertical displacement to horizontal displacement from MTS machine registration.
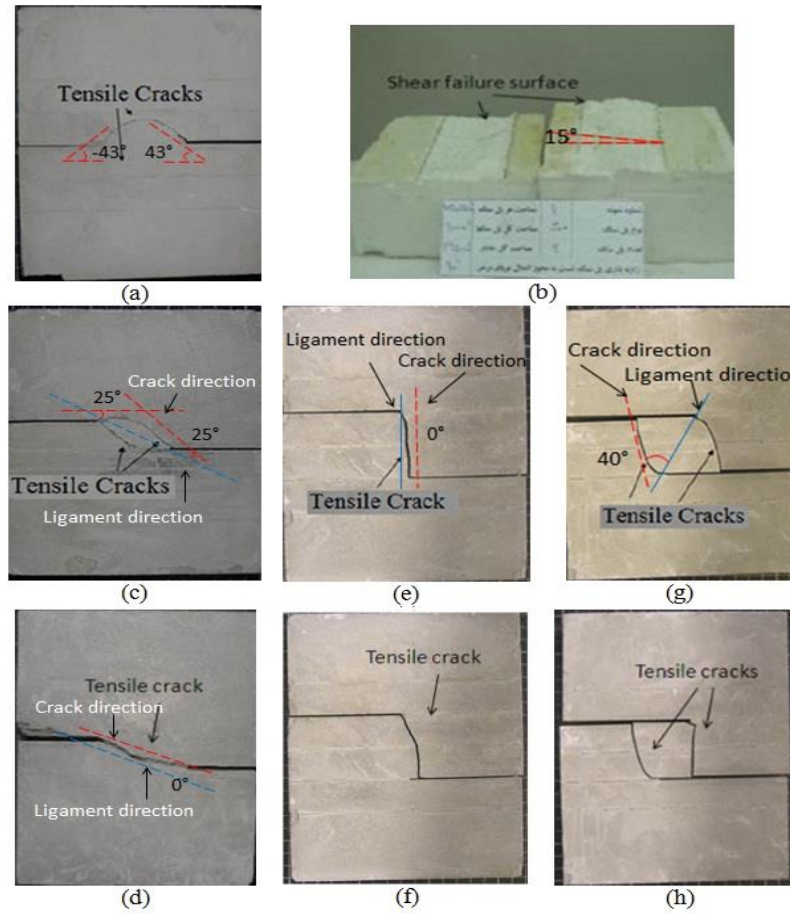
Fig. 3 Failure patterns obtained in the direction of shear tests

Table 2 micro properties used to represent the intact rock

Parameter	Value	Parameter	Value
Type of particle	Disc	Parallel bond radius multiplier	1
density	3000	Young modulus of parallel bond (GPa)	40
Minimum radius	0.27	Parallel bond stiffness ratio	1.7
Size ratio	1.56	Particle friction coefficient	0.4
Porosity ratio	0.08	Parallel bond normal strength, mean (MPa)	8
Damping coefficient	0.7	Parallel bond normal strength, SD (MPa)	2
Contact young modulus (GPa)	40	Parallel bond shear strength, mean (MPa)	8
Stiffness ratio	1.7	Parallel bond shear strength, SD (MPa)	2

Under high normal loading (Fig. 3(b)), the uneven shear crack propagates through the intact portion area. In these failure patterns, the failure surface in bridge area is shear because the crushed or pulverized materials and the evidence of shear movement were noticed along the shear surface. Mean orientation of shear surface related to ligament direction was nearly 15°. Dilation angle in this configuration was close to 13°.

When the ligament angle is 25°, under low normal load (Fig. 3(c)), the wing cracks initiate at the tips of the joints and propagate in a curvilinear path until they coalesce with

the tips of other joints. This coalescence leave an elliptical core completely separated from the sample. Failure surface in the bridge area is tensile because there were no crushed or pulverized materials and no evidence of shear movement noticed along the failure surface. Mean orientation of shear surface related to ligament direction is around 25°. Dilation angle in this configuration is 11°.

Under high normal load (Fig. 3(d)), the shear cracks initiate at the tips of the joints and propagate in a diagonal path with respect to shear load direction, 25°, until the cracks coalesce with each other. This coalescence leave two blocks completely separated from each other. Failure surface in bridge area is shear because there were no crushed or pulverized materials and no evidence of shear movement noticed along the shear surface. Mean orientation of shear surface related to ligament direction is about 0°. Dilation angle in this configuration is close to 7°.

When the ligament angle is 90°, under low normal load (Fig. 3(e)), the tensile crack initiates at the tips of the joints and propagates through the bridged segment. In this configuration, the rock bridge is broken with a single failure surface. Mean orientation of shear surface related to ligament direction is around 0°. Dilation angle in this configuration is 0°.

Under high normal load (Fig. 3(f)), the rock bridge failure occurs under normal loading. In this condition the tensile crack initiate at the upper joint tip and propagate parallel to normal load direction till coalesce with the lower

Table 3 Macro-mechanical properties of model material in experimental tests and PFC2D, Ghazvinian *et al.* (2012)

Mechanical Properties	Experimental results	PFC2D model results	Mechanical properties	Experimental results	PFC2D model results
Elastic modulus (GPa)	5.4	5	Tensile strength	1	1.1
Poisson's ratio	0.18	0.19	Friction angle	20.4	21
UCS(MPa)	6.6	6.7	Cohesion (MPa)	2.2	2.2

joint wall. Failure surface in the bridge area is tensile because there were no crushed or pulverized materials and no evidence of shear movement noticed along the failure surface.

When the ligament angle is 115°, under low normal load (Fig. 3(g)), the wing cracks initiate at the joint walls and develop nearly in a vertical direction. These wing cracks propagate through the intact portion area until they coalesce with the opposite joints tips. This coalescence leave a rectangular core of intact material completely separated from the sample. In these failure patterns, the failure surface in bridge area is tensile because there were no crushed or pulverized materials and no evidence of shear movement noticed along the cracks. Mean orientation of shear surface related to ligament direction is close to 0°. Dilation angle in this configuration is 0°.

Under high normal load (Fig. 3(h)), rock bridge failure occurs under normal loading. In this condition the tensile crack initiate at the tips of the joints and propagate nearly parallel to normal load direction, 115°, till coalesce with the lower joint wall. Failure surface in bridge area is tensile because there were no crushed or pulverized materials and no evidence of shear movement noticed along the failure surface. It can be concluded from the above discussions that, dilation angle is decreasing by increasing the ligament angle and the normal loading.

3. Numerical modelling with PFC2D

Particle flow code represents a rock mass as an assemblage of bonded rigid particles (Potyondy and Cundall 2004). In the two dimensional version (PFC2D), circular disks are connected with cohesive and frictional bonds (bond strength) and confined with planar walls. Parallel bond model was adopted in this study to simulate the contacts between particles. The values assigned to strength bonds influence the macro strength of a sample and the nature of cracking and failure. Friction is activated by specifying the coefficient of friction and is mobilized as long as particles stay in contact. Tensile cracks occur when the applied normal stress exceeds the specified normal bond strength. Shear cracks are generated as the applied shear stress exceeds specified shear bond strength either by rotation or shearing the particles. Tensile strength at contact drops immediately to zero after the bond breaks, while shear strength decreases to residual friction value (Itasca Consulting Group Inc 2004, Cho *et al.* 2007, 2008, Potyondy and Cundall 2004). For all these microscopic behaviours, PFC only requires selection of the basic micro-parameters to describe contact and bond stiffness, bond strength and contact friction, but these micro-parameters should provide the macro-scale behaviour of the material

being modelled. The code uses an explicit finite difference scheme to solve the equation of force and motion, and hence one can readily track initiation and propagation of bond breakage (fracture formation) through the system (Potyondy and Cundall, 2004).

3.1 Preparation and calibration of the PFC2D model for rock-like material

The standard process of generating a PFC2D assembly to represent a test model, used in this article, is described in detail by Itasca (2004). The process involves: particle generation, packing the particles, isotropic stress installation (stress initialization), floating particle (floater) elimination and bond installation. A gravity effect did not need to be considered as the specimens were small, and the gravity-induced stress gradient had a negligible effect on macroscopic behaviors.

Uniaxial compressive strength, Brazilian and biaxial tests were carried out to calibrate the properties of particles and the parallel bonds in bonded particle model (Sarfarazi *et al.* 2014). By adopting the micro-properties listed in Table 2 and the standard calibration procedures (Potyondy and Cundall 2004), a calibrated PFC particle assembly was created.

Different numerical simulations and experimental tests was considered for model calibration and summarized in the following sections:

3.2 Numerical unconfined compressive test

A comparison between numerical results and experimental measurements are presented in Table 3.

3.3 Brazilian test

Numerical tensile strength and experimental measurements and presented in Table 3. A comparison of the Brazilian experimental measurements given in Table 3 shows good agreements with those of the numerical results.

3.4 Biaxial test

A comparison of tri-axial experimental results given in Table 3 demonstrates suitably good agreement with those of the numerical.

3.5 Numerical direct shear tests on the non-persistent open joint

3.5.1 Preparing the model
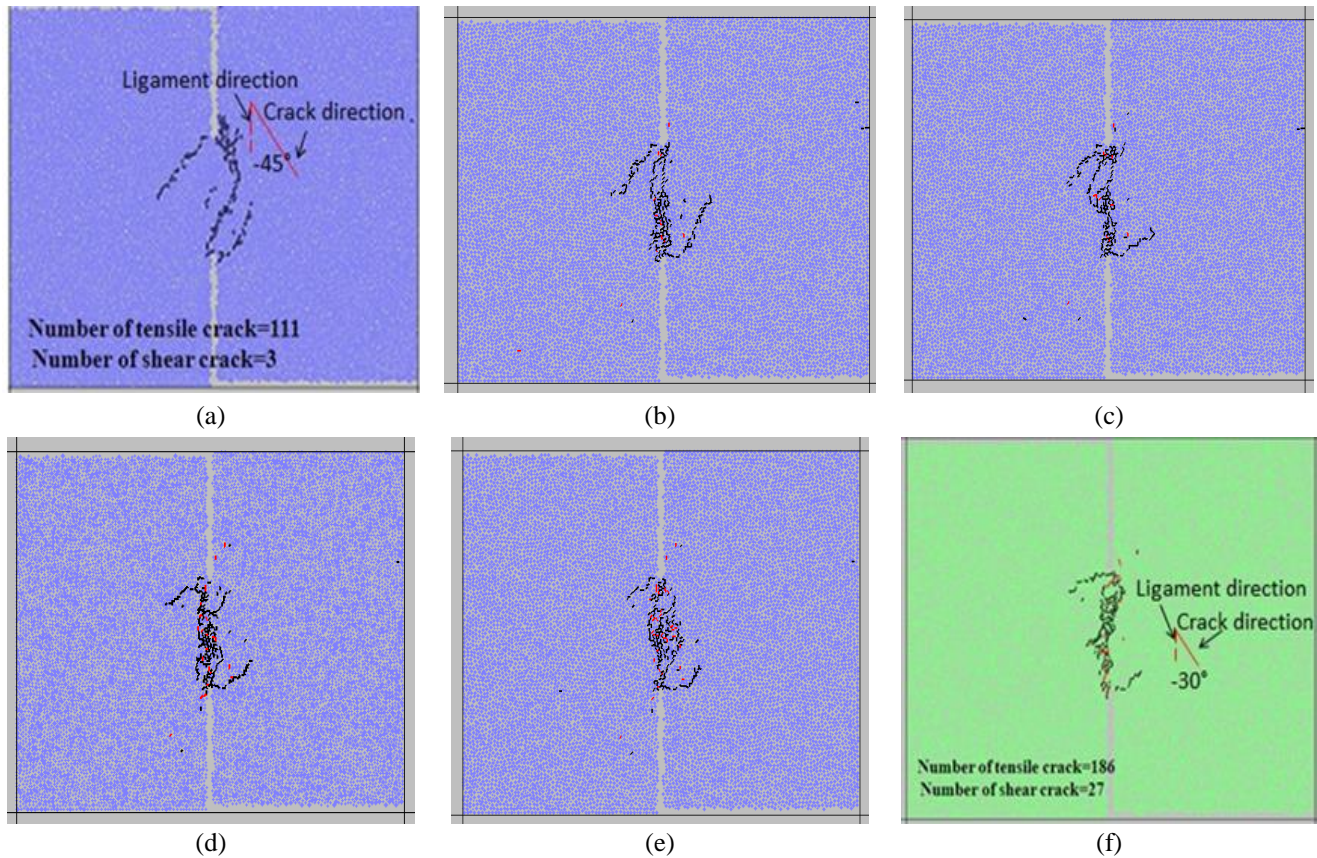After calibration of PFC2D, direct shear tests for jointed

Fig. 4 Development of cracks and mean orientation of particle cracks under normal stress of, (a) 0.3 MPa, (b) 0.7 MPa, (c) 1 MPa, (d) 1.5 MPa, (e) 2 MPa and (f) 2.5 MPa

rock were numerically simulated by creating a shear box model in the PFC2D. The specifications of PFC specimen were introduced in details by Sarfarazi *et al.* (2012). In total, seven specimens containing two planar edge-notched joints with different ligament angels were set up to investigate the influence of ligament angle on shear behaviour of rock bridges. For different specimens, the lengths of these edge-notched joints were different, while in the same specimen, the lengths of those two joints were the same. The joint lengths (b) are 2.1, 2.18, 2.42, 2.76, 3, 3.38 and 3.69 mm that are associated with ligament angles of 0°, 25°, 50°, 90°, 115° and 140°, respectively.

3.5.2 Loading set up

Both, upper and left walls of shear box were fixed in X and Y directions. Shear loading was applied to sample by moving the lower wall in Y-direction, with an adequate low velocity (i.e., 0.016 m/s) to ensure a quasi-static equilibrium, while the normal stress was kept constant by adjusting the velocity of right wall using a numerical servo-mechanism.

Normal stresses applied to the rock bridges in the numerical simulations were 0.3 MPa, 0.7 MPa, 1 MPa, 1.5 MPa, 2 MPa and 2.5 MPa). Normal stresses of 0.3 MPa and 2.5 MPa are similar in both of the numerical model and experimental sample. Shear displacement was measured by tracing the lower wall displacement. The shear force was registered by taking the reaction forces on the wall. Each test takes 15 min to run.

4. Results and discussion

4.1 Influence of normal load on the failure behaviour of the rock bridge

Figs. 4, 5, 6, 7, 8 and 9 illustrate the shear behaviours of rock bridges under two different normal loads for ligament angles of 0°, 25°, 50°, 90°, 115° and 140°, respectively. In each figure, the fracture patterns at three stages of shear loading (i.e., at the crack initiation stress stage of I, at the peak stress of II, and after the peak shear stress of III) was shown. At each stage of simulation, the crack orientation related to the ligament direction and the number of shear and tension induced cracks were determined.

4.1.1 Ligament angles is 0°

When normal load is 0.3 MPa (Fig. 4(a)), new cracks develop in the rock bridge and coalesce at joint tips so that the intact bridge area becomes split with an uneven shear failure surface.

Mean orientation of these cracks in respect to ligament direction is -45°. Dilation angle in this configuration is 19°. Number of tensile cracks is 37 times more than the shear cracks.

The length and orientation of upper and lower wing cracks stay unchanged after stage (a). This means that shear loading has no effect on force concentration near the wing cracks after first stage.
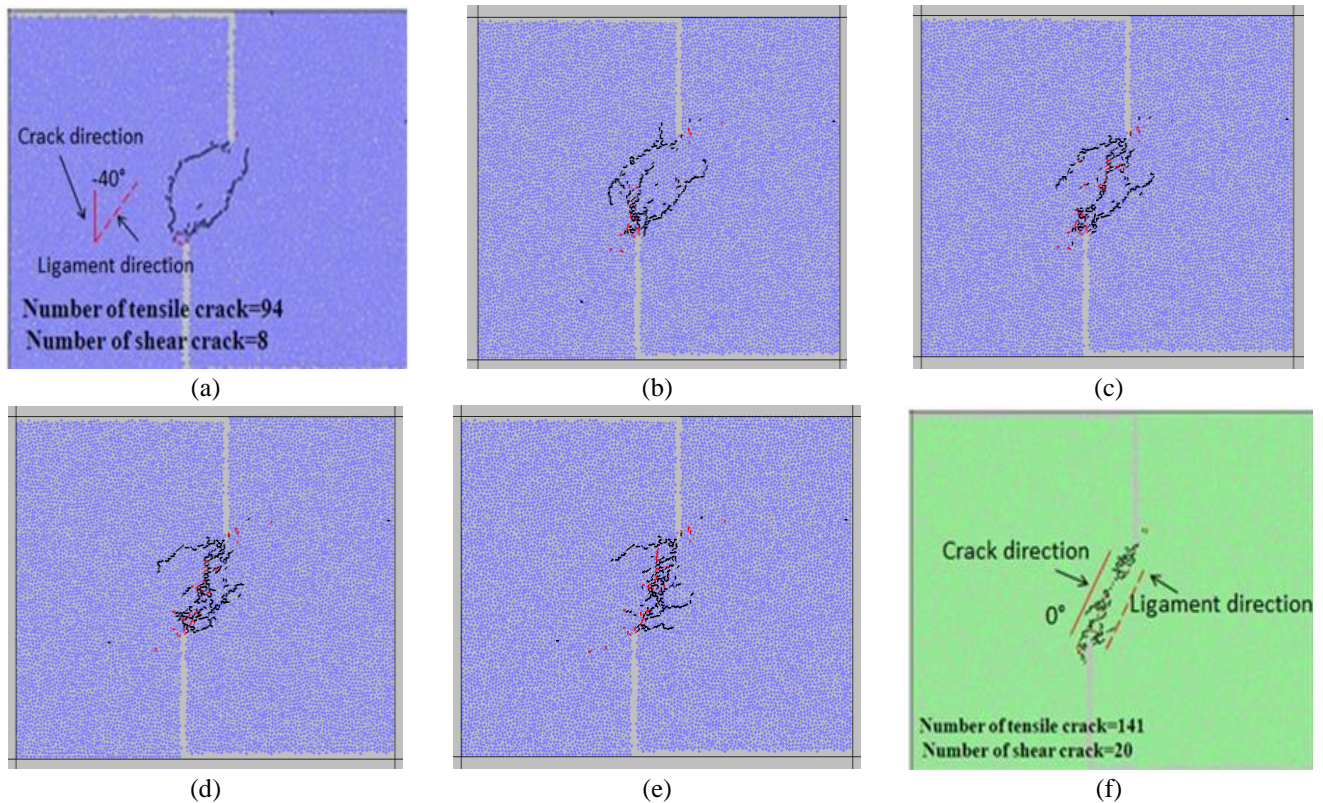
Fig. 5 Development of cracks and mean orientation of particle cracks under normal stress of, (a) 0.3 MPa, (b) 0.7 MPa, (c) 1 MPa, (d)1.5 MPa, (e) 2 MPa and (f) 2.5 MPa

As it can be seen from Fig. 3(a), nearly the same failure pattern occurred in physical sample when the ligament angle was 0°. As for the other numerical samples in this part, the failure patterns obtained by simulation are in reasonable agreement within some related experimental results reported by Wong and Chau (1998), (2002) and Zhang (2006). When normal load is 2.5 MPa (Fig. 4(f)), several shear bands develop within the rock bridge and propagates with a mean orientation of 40°. Also, the new tensile cracks develop between the shear bands with a mean orientation of -30°. Therefore the intact bridge area gets split with an uneven shear failure surface. The number of tensile cracks is 7 times more than shear crack numbers. The dilation angle in this configuration is 9°.

The length and orientation of first type of tensile cracks remain constant after the first stage of shear loading. It means that the external shear load does not induce any force concentration near these cracks during the different stages of shear loading (stages of I and II).

As can be seen from Fig. 3(b), nearly the same failure pattern occurred in the physical sample when the ligament angle was 0°. As for the other numerical samples in this part, the failure patterns obtained from this simulation are in reasonable agreement with some of the related experimental results reported by Wong and Chau (1998), Wong *et al.* (2001).

4.4.2 Ligament angle is 25°

When normal load is 0.3 MPa (Fig. 5(a)), the upper and the lower wing cracks propagate within the rock bridge until they coalesce with the opposite joint tip. This coalescence leaves an elliptical segment. Mean orientation of these cracks in respect to ligament direction is -40°. Dilation angle in this configuration is 13°. Number of tensile cracks is 12 times more than total shear cracks. As it can be seen from Fig. 3(c), same failure pattern occurred for physical samples when the ligament angle was 25°.

When normal load is 2.5 MPa (Fig. 5(f)), the new cracks develop within the rock bridge until they coalesce with pre-existing shear bands. Mean orientation of these cracks is 0°. Dilation angle in this configuration is 3°. Number of tensile cracks is 7 times more than shear crack numbers. It shows that the tensile fracturing is dominant mode of failure which occurs within the rock bridge.

As can be seen from Fig. 3(d), the same failure pattern occurred in the physical samples when the ligament angle was 25°.

4.4.3 Ligament angle is 50°

When normal load is 0.3 MPa (Fig. 6(a)), the upper and the lower wing cracks propagate within the Rock bridge until they coalesce with the opposite joint tips. This coalescence leaves an elliptical core. Mean orientation of these cracks with respect to ligament direction is -20°. Dilation angle in this configuration is 5°. Number of tensile cracks is 24 times more than of shear cracks. It shows that, tensile fracturing is the dominant mode of failure occurring within the rock bridges.

When normal load is 2.5 MPa (Fig. 6(f)), the upper and the lower wing cracks propagate within the rock bridge
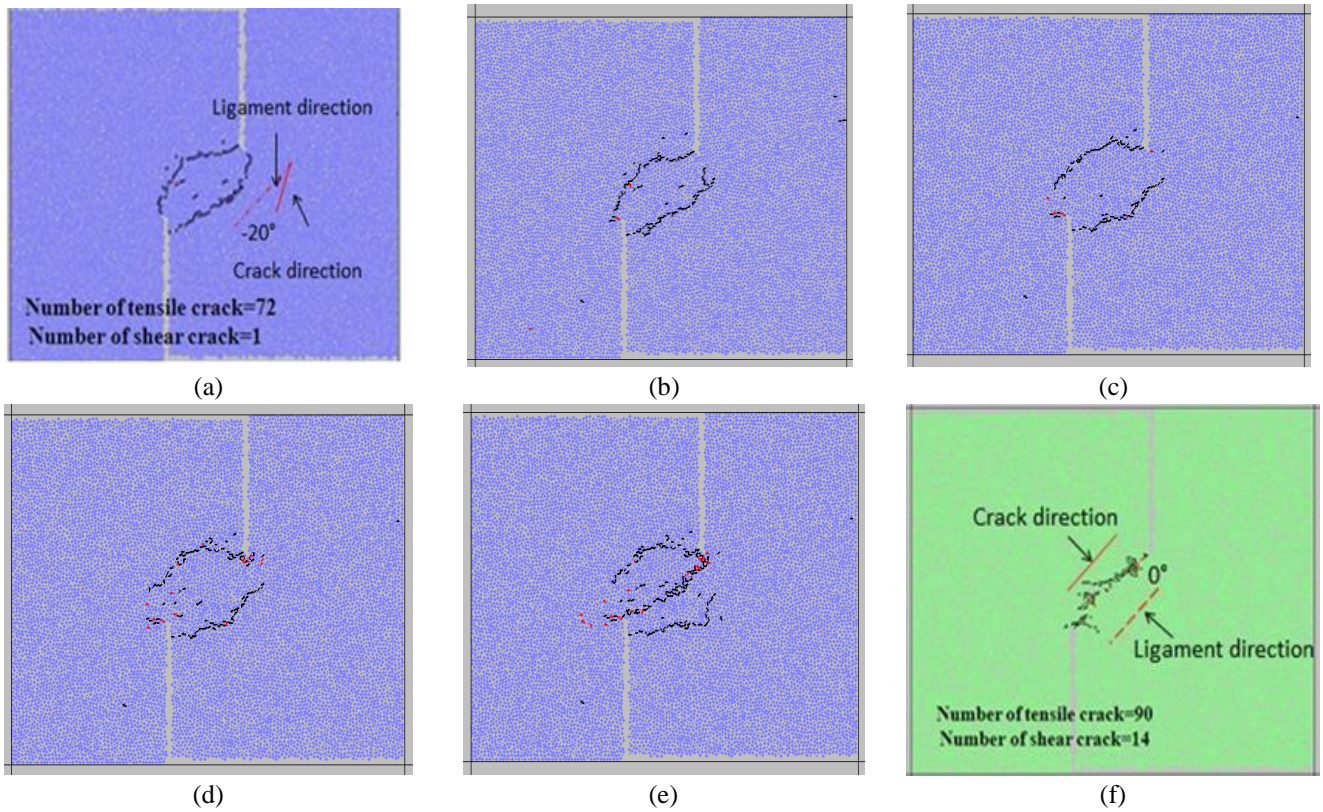
Fig. 6 Development of cracks and mean orientation of particle cracks under normal stress of, (a) 0.3 MPa, (b) 0.7 MPa, (c) 1 MPa, (d)1.5 MPa, (e) 2 MPa and (f) 2.5 MPa

until they coalesce with each other. Number of tensile cracks is 6.4 times more than that of shear cracks. It shows that, tensile fracturing is the dominant mode of failure occurring within the rock bridges. Mean orientation of failure surface is 0°. Dilation angle in this configuration is 1°.

4.4.4 Ligament angle is 90°

When normal load is 0.3 MPa (Fig. 7(a)), both the upper and lower wing cracks propagate through the intact portion until they coalesce with the opposite joint tips. Mean orientation of these cracks with respect to ligament direction is 0°.

Dilation angle in this configuration is 0°. Number of tensile cracks is 42 times more than that of shear cracks. It shows that the tensile fracturing is the dominant mode of failure occurring within the rock bridge. As it can be seen from Fig. 3(f), nearly the same failure pattern occurred in physical samples when the ligament angle was 90°. When normal load is 2.5 MPa (Fig 6(f)), the wing cracks initiate from joint tip and propagate within the rock bridge till coalesce with each other.

4.4.5 Ligament angle is 115°

Stage I: When normal load is 0.3 MPa (Fig. 8(a) (I)), almost no crack initiated within the rock bridge. When normal load is 2.5 MPa, failure of Rock Bridge occurs under normal loading (Fig. 8(b)). In this configuration, tensile cracks initiate from the joint tips and propagate parallel to the normal load direction till coalesce with each other. As it

can be seen from Fig. 3(g), nearly the same failure pattern occurred in physical samples when the ligament angle was 115°.

Stage II: When normal load is 0.3 MPa (Fig. 8(a) (II)), the lower wing cracks develop from the wall of the lower joint. Mean orientation of these cracks is nearly 0°.

In this loading stage, nearly 8% of total cracks develop stably at the rock bridge. It means that, the rock bridge loses its loading capacity when 8 % of total cracks develop within. Fig. 3(f), nearly the same failure pattern occurred in physical samples when the ligament angle was 115°.

Stage III: When normal load is 0.3 MPa (Fig. 8(a) (III)), both the upper and the lower wing cracks propagate through the intact portion area until they coalesce with the opposite joint tips. This failure leave an elliptical core completely separated from the model. Mean orientation of these cracks with respect to ligament direction is 0°. Dilation angle in this configuration is 0°. Number of tensile cracks is 40 times higher than that of shear cracks. It shows that, the tensile fracturing is the dominant mode of failure occurring within the rock bridge. As it can be seen from Fig. 3(h), nearly the same failure pattern occurred in physical samples when the ligament angle was 115°. It's to be note that the model breakage occurs under normal load when it is high (Fig. 8(b)).

4.4.6 Ligament angle is 140°

Stage I: When normal load is 0.3 MPa (Fig. 9(a) (I)), Almost no crack initiated within the rock bridge. When normal load is 2.5 MPa, failure of Rock Bridge occurs under
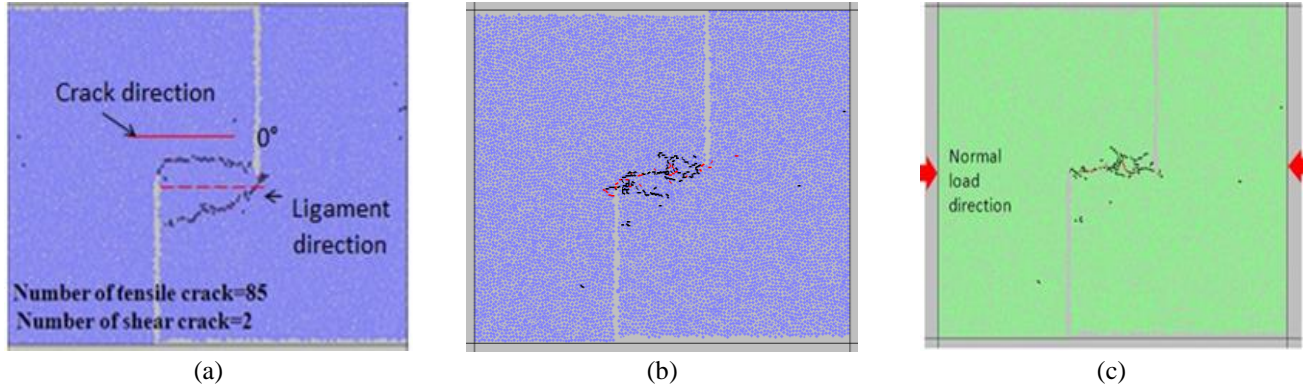
Fig. 7 Development of cracks and mean orientation of particle cracks under normal stress of, (a) 0.3 MPa, (b) 0.7 MPa, (c) 1 MPa
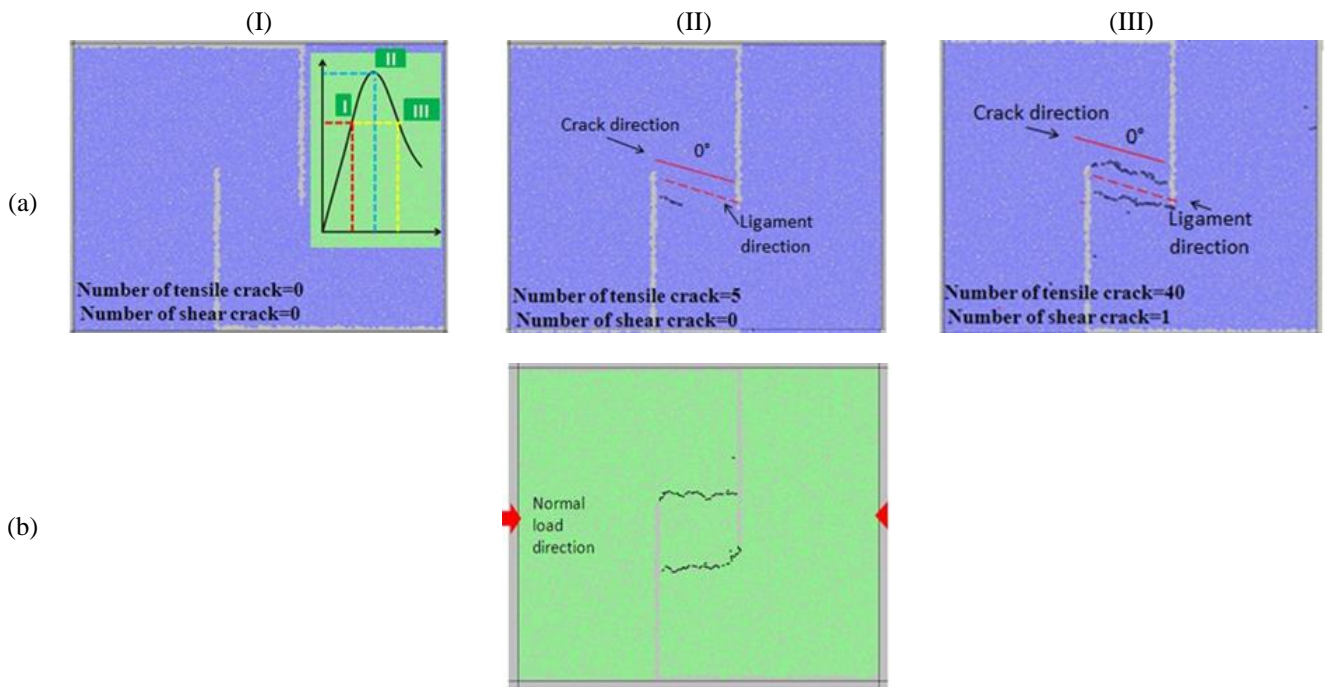

Fig. 8 Development of cracks and mean orientation of particle cracks during the three stages of shear loading of (I), (II) and (III); (a) under low normal load of 0.3 MPa, (b) under high normal load of 2.5 MPa

normal loading (Fig. 9(b)). In this configuration, tensile cracks initiate at joint tips and propagate parallel to normal load direction till coalesce with each other.

Stage II: When normal load is 0.3 MPa (Fig. 9(a) (II)), the upper wing cracks develop from the wall of the joint. Mean orientation of these cracks is near to 45°. In this loading stage, nearly 9 % of the total cracks develop stably in the rock bridge. It means that, the rock bridge loses its loadingcapacity when 9 % of total cracks develop within.

Stage III: When normal load is 0.3 MPa (Fig. 9(a) (III)) the wing crack propagates perpendicular to shear loading direction until it coalesces with the opposite joint tip.

Mean orientation of these cracks with respect to ligament direction is 45°. Dilation angle in this configuration is 0°. Number of tensile cracks is 20 times higher than that of shear cracks. It shows that the tensile fracturing is the dominant mode of failure occurring within.

It's to be note that the model breakage occurs under

normal load when it is high (Fig. 9(b)).

From the above discussions, generally we can conclude that the failure pattern has a close relationship with both, ligament angle and normal loading.

For a ligament angle of 0°, the intact-bridged rock ruptures in "v" shape mode under low normal loading, but the intact-bridged rock ruptures with several shear bands under high normal loading. When ligament angle is 25°, the middle bridged rock ruptures in "fish eye" mode with two narrow shear failure surfaces under low normal loading, but the bridged rock ruptures in "thicken line" mode with several short shear bands under high normal loading. when ligament angle is 50°, the middle bridged rock ruptures in "fish eye" mode with two narrow shear failure surfaces under low normal loading, but the bridged rock ruptures in "thicken line" mode with several short shear bands under high normal loading. When ligament angle is 90°, the joints are connected by two horizontal wing cracks under low
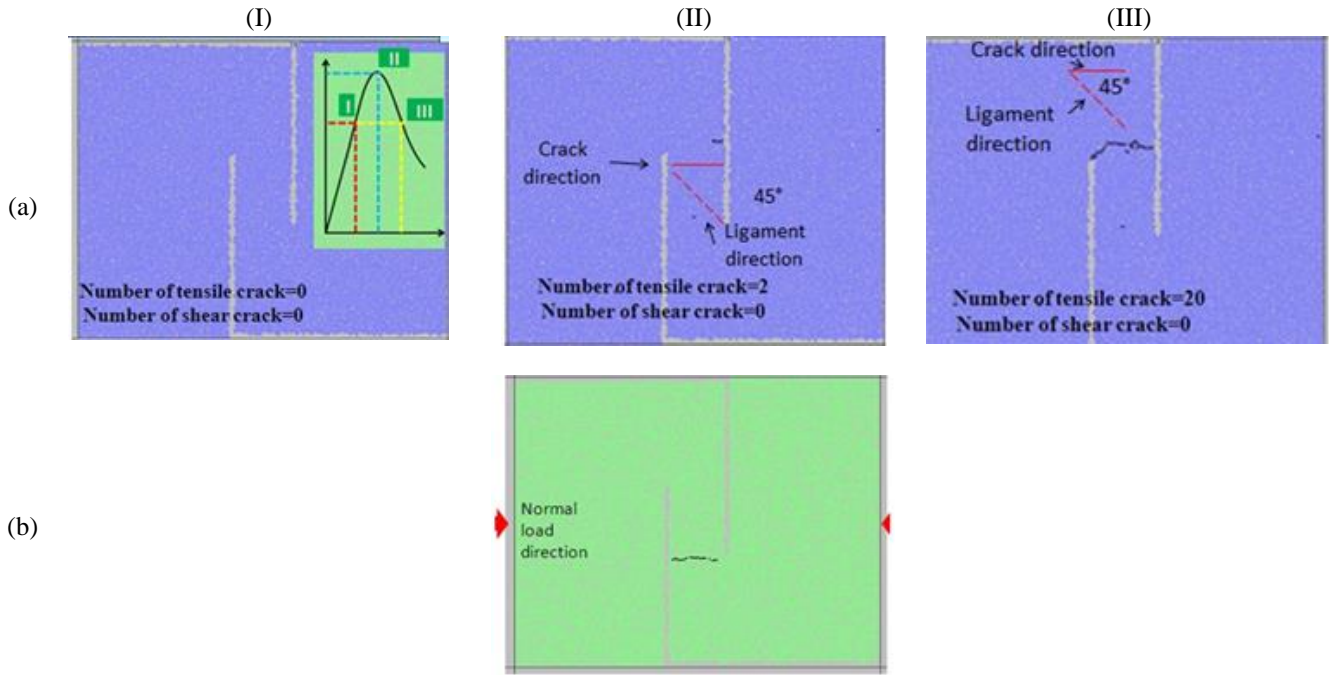
Fig. 9 Development of cracks and mean orientation of particle cracks during the three stages of shear loading of I, II and III; (a) under low normal load of 0.3 MPa, (b) under high normal load of 2.5 MPa
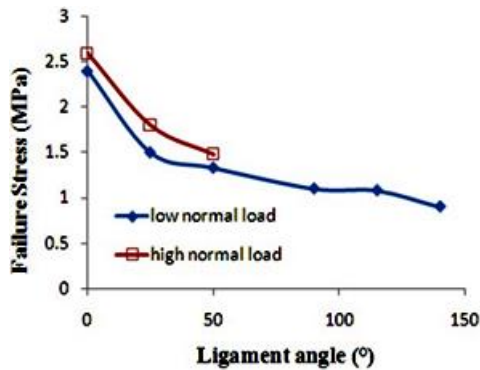

Fig. 10 The variation of failure stresses versus the ligament angle for normal loads of 0.3 MPa and 2.5 MPa

normal loading, but the shear failure is not occurring under any high normal loadings. When ligament angle is 115°, the joints are connected by two diagonal wing cracks under low normal loading, but the shear failure is not occurring under any high normal loadings. Finally, for ligament angle of 140°, the joints are connected by one horizontal wing crack under low normal loading, but the shear failure is not occurring under any high normal loadings.

The results show that, in fixed ligament angle, the mean orientation of cracks with respect to ligament direction is decreased by increasing the normal load. Similarly, dilation angle is decreased by increasing the normal load similar to that observed in experimental test. Dilation angle was reduced by increasing the ligament angle too.

In low normal loading, the mean orientation of crack propagation with respect to ligament direction was decreased by increasing the ligament angel. But in high normal loading, the mean orientation of crack propagation with respect to ligament direction is nearly stayed constant when

ligament angel was increased.

Fig. 10 shows the variation of numerical failure stresses versus ligament angle. Failure stress is measured by diving related force to the rock bridge surface area. Because the models have a unit thickness, the rock bridge area is equal to the ligament length. The fill points and the hollow points are representing the stresses under two different normal loadings of 0.3 MPa and 2.5 MPa, respectively.

From Fig. 10 we can conclude that the capacity of bridged rock to resist shear loading has a close relationship with both, the ligament angle and the normal load.

Failure stress was decreased by decreasing normal load. In fact, in fixed ligament angle, induced tensile force on the rock bridge was decreased by increasing the normal load. This leads to increasing the failure stress. Also, the more the ligament angle is, the less the failure stress is. Generally in fixed normal loading, the induced tensile force on the rock bridge is increased by increasing the ligament angle. This leads to failure stress reduction.

Fig. 11(a) and (b) show the variation of failure stresses, for both numerical and experimental tests, versus the ligament angle under two different normal loadings of 0.3 MPa and 2.5 MPa, respectively. Fill points and hollow points are representing the stresses for PFC2D models and laboratory samples, respectively. Fig. 11(c) and (d) represent the variation of failure stress and crack initiation stress versus ligament angle for low and high normal loadings, respectively. Crack initiation stress is defined as a stress where 8% of total cracks are initiated. Fig. 11(a) and (b) shows that the shear strength of non-persistent joints predicted by numerical simulations are nearly similar to the results obtained by experimental tests. Slight discrepancy may be due to some small variations in mechanical specifications of numerical and laboratory specimens (i.e.,
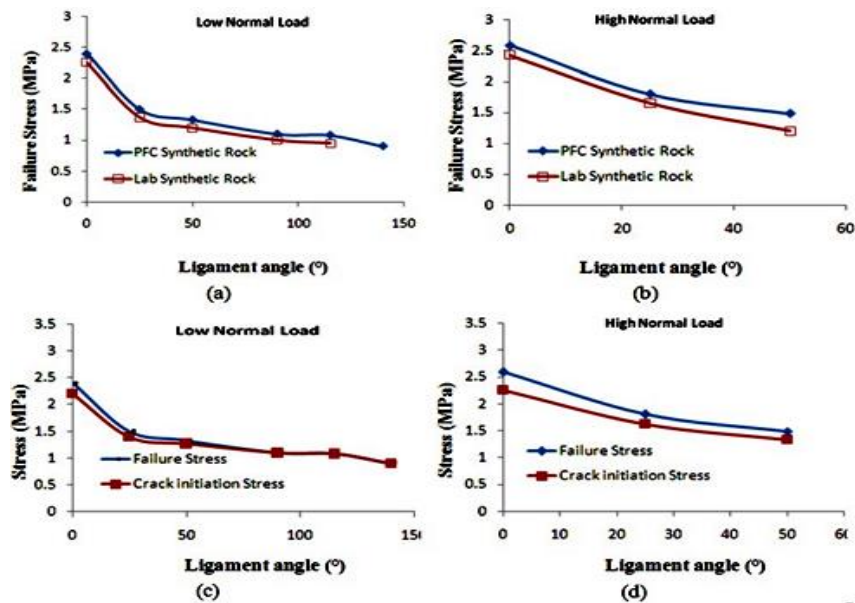
Fig. 11 (a) the variation of failure stresses versus the ligament angle for normal loads of 0.3 MPa, (b) the variation of failure stresses versus the ligament angle for normal loads of 2.5 MPa, (c) the variation of failure/crack initiation stress versus the ligament angle under low normal load and (d) the variation of failure/crack initiation stress versus the ligament angle under high normal load

tensile strength and friction angle given in Table 2).

From Fig. 11(c) and (d), the crack initiation stress is decreasing by increasing the ligament angle. When normal load is 0.3 MPa, difference between failure stress and crack initiation stress is low (Fig. 11(c)) i.e., and brittle failure occurs in the rock bridge. But when normal load is 2.5 MPa, the difference between failure stress and crack initiation stress will be high (Fig. 11(d)) i.e., and progressive failure occurs in rock bridge. This means that, the brittle failure changes to progressive failure by increasing normal load.

Finally, it may be concluded that the shear loading peak for jointed rock was mostly influenced by its failure pattern, while the failure pattern of bridged rock was mainly controlled by the normal load. Whereas shear strength, as one of the material mechanical properties has a close relationship with normal loading, the capacity of jointed rock masses to resist shear loading was severely influenced by stress distribution around the rock masses.

5. Conclusions

Laboratory experiments and numerical simulations reported in this paper show that, the dominant mode of fracture irrespective of any shear stages is tensile. Also, numerical simulation of the synthetic rock showed that the fracture patterns are similar to those observed experimentally.

• When normal load increases from 0.3 to 2.5 MPa, number of shear cracks increases while tensile cracking would be the dominant mode of failure occurring in the rock bridge.

• In fixed ligament angle, increasing the normal loading from 0.3 to 2.5 MPa, will increase the number of cracks. This shows that, fracturing intensity was increased by increasing the normal loading.

• In fixed ligament angle, mean orientation of crack propagation with respect to ligament direction decreased by increasing normal loading.

• In fixed ligament angle, the symmetrical "fish eye" failure pattern changed to a linear failure pattern by increasing the normal loading.

• For ligament angle of less than 90°, the stable crack growth length increases by increasing the normal loading. For higher than 90°, the rock bridge breaks under large normal loading.

• In low normal loading, mean orientation of crack propagation with respect to ligament direction decreases by increasing the ligament angel. But for high normal loading, mean orientation of crack propagation with respect to ligament direction stays nearly constant by increasing the ligament angel.

• In fixed ligament angle, dilation angle decreases by increasing the normal loading.

• In fixed normal loading, dilation angle decreases by increasing the ligament angle.

References

Bahaaddini, M., Sharrock, G. and Hebblewhite, B.K. (2013), "Numerical investigation of the effect of joint geometrical parameters on the mechanical properties of a non-persistent jointed rock mass under uniaxial compression", *Comput. Geotech.*, **49**, 206-225.

Bazant, Z.P., Tabbara, M.R., Kazemi, M.T. and Gilles, P.C. (1990), "Random particle model for fracture of aggregate or fiber composites", *J. Eng. Mech.*, ASCE, **116**(8), 1686-1705.

Bobet, A. and Einstein, H.H. (1998), "Fracture coalescence in rock-type materials under uniaxial and biaxial compression", *J. Rock Mech. Min. Sci.*, **35**(7), 863-888.

Cho, N., Martin, C.D. and Sego, D.C. (2007), "A clumped particle

model for rock", *J. Rock Mech. Min. Sci.*, **44**(7), 997-1010.

Cho, N., Martin, C.D. and Sego, D.C. (2008), "Development of a shear zone in brittle rock subjected to direct shear", *J. Rock Mech. Min. Sci.*, **45**(8), 1335-1346.

Gehle, C. and Kutter, H.K. (2003), "Breakage and shear behavior of intermittent rock joints", *J. Rock Mech. Min. Sci.*, **40**(5), 687-700.

Ghazvinian, A., Nikudel, M.R. and Sarfarazi, V. (2007), *Effect of Rock Bridge Continuity and Area on Shear Behavior of Joints*, 11th Congress of the International Society for Rock Mechanics, Lisbon, Portugal.

Ghazvinian, A., Sarfarazi, V., Schubert, W. and Blumel, M. (2012), "A study of the failure mechanism of planar non-persistent open joints using PFC2D", *Rock Mech. Rock Eng.*, **45**(5), 677-693.

Haeri, H. (2011), "Numerical modeling of the interaction between micro and macro cracks in the rock fracture mechanism using displacement discontinuity method", Ph.D. Dissertation, Department of Mining Engineering, Science and Research Branch, Islamic Azad University, Tehran, Iran.

Haeri, H. (2015d), "Propagation mechanism of neighboring cracks in rock-like cylindrical specimens under uniaxial compression", *J. Min. Sci.*, **51**(3), 487-496.

Haeri, H. (2015e), "Influence of the inclined edge notches on the shear-fracture behavior in edge-notched beam specimens", *Comput. Concrete*, **16**(4), 605-623.

Haeri, H. (2015f), "Experimental crack analysis of rock-like CSCBD specimens using a higher order DDM", *Comput. Concrete*, **16**(6), 881-896.

Haeri, H. and Ahranjani, A.K. (2012), "A fuzzy logic model to Predict crack propagation angle under Disc Cutters of TBM", *J. Academic Res.*, **4**(3), 156-169.

Haeri, H. and Sarfarazi, V. (2016), "The effect of micro pore on the characteristics of crack tip plastic zone in concrete", *Comput. Concrete*, **17**(1), 107-112.

Haeri, H., Khaloo, K. and Marji, M.F. (2015b), "Experimental and numerical analysis of Brazilian discs with multiple parallel cracks", *Arabian J. Geosci.*, **8**(8), 5897-5908

Haeri, H., Marji, M.F. and Shahriar, K. (2015a), "Simulating the effect of disc erosion in TBM disc cutters by a semi-infinite DDM", *Arabian J. Geosci.*, **8**(6), 3915-3927.

Haeri, H., Shahriar, K., Marji, M.F. and Moarefvand, P. (2013a), "Modeling the propagation mechanism of two random micro cracks in rock samples under uniform tensile loading", *Proceedings of the 13th International Conference on Fracture*, China.

Haeri, H., Shahriar, K., Marji, M.F. and Moarefvand, P. (2013b), "Simulating the bluntness of TBM disc cutters in rocks using displacement discontinuity method", *Proceedings of the 13th International Conference on Fracture*, China.

Haeri, H., Shahriar, K., Marji, M.F. and Moarefvand, P. (2014a), "On the cracks coalescence mechanism and cracks propagation paths in rock-like specimens containing pre-existing random cracks under compression", *J. Central South Univ.*, **21**(6), 2404-2414.

Haeri, H., Shahriar, K., Marji, M.F. and Moarefvand, P. (2014b), "Investigating the fracturing process of rock-like Brazilian discs containing three parallel cracks under compressive line loading", *Strength Mater.*, **46**(3), 133-148.

Haeri, H., Shahriar, K., Marji, M.F. and Moarefvand, P. (2015c), "The HDD analysis of micro cracks initiation, propagation and coalescence in brittle substances", *Arabian J. Geosci.*, **8**(5), 2841-2852.

Itasca Consulting Group Inc (2004), "Particle flow code in 2-dimensions (PFC2D)", Minneapolis.

Jaeger, J.C. (1971), "Friction of rocks and stability of rock slopes", *Geotech.*, **21**(2), 97-134.

Jiang, S., Du, C. and Gu, C. (2014), "An investigation into the effects of voids, inclusions and minor cracks on major crack propagation by using XFEM", *Struct. Eng. Mech.*, **49**(5), 597-618.

Kumar, S. and Barai, S.V. (2012), "Size-effect of fracture parameters for crack propagation in concrete: A comparative study", *Comput. Concrete*, **9**(1), 1-19.

Li, Y.P., Chen, L.Z. and Wang, Y.H. (2005), "Experimental research on pre-cracked marble", *J. Solid. Struct.*, **42**(9), 2505-2016.

Mohamed, A.R. and Hansen, W. (1999), "Micromechanical modelling of concrete response under static loading-Part I: Model development and validation", *ACI Mater. J.*, **96**(2), 196-203.

Mughieda, O. and Alzo'ubi, A.K. (2004), "Fracture mechanisms of offset rock joints-A laboratory investigation", *Geotech. Geol. Eng.*, **22**(4), 545-562.

Mughieda, O. and Karasneh, I. (2006), "Coalescence of offset rock joints under biaxial loading", *Geotech. Geol. Eng.*, **24**(4), 985-999.

Mughieda, O.S. and Khawaldeh, I. (2004), "Scale effect on engineering properties of open non-persistent rock joints under uniaxial loading", *Proceedings of the 7th Regional Rock Mechanics Symposium*, Sivas, Turkey.

Olson, J.E. and Pollard, D.D. (1991), "The initiation and growth of en-echelon veins", *J. Struct. Geol.*, **13**(5), 595-608.

Potyondy, D.O. and Cundall, P.A. (2004), "A bonded-particle model for rock", *J. Rock Mech. Min. Sci.*, **41**(8), 1329-1364.

Sagong, M. and Bobet, A. (2002), "Coalescence of multiple flaws in a rock model material in uniaxial compression", *J. Rock Mech. Min. Sci.*, **39**(2), 229-241.

Sarfarazi, V., Ghazvinian, A., Schubert, W., Blumel, M. and Nejati, H.R. (2014), "Numerical simulation of the process of fracture of echelon rock joints", *Rock Mech. Rock Eng.*, **47**(4), 1355-1371.

Sarfarazi, V., Haeri, H. and Khaloo, A. (2016), "The effect of non-persistent joints on sliding direction of rock slopes", *Comput. Concrete*, **17**(6), 723-737.

Vonk, R.A., Rutten, H.S., Van Mier, J.G.M. and Funeman, H.J. (1991), "Micromechanical simulation of concrete softening", *Proceedings of the International RILEM/ESIS Conference Fracture Processes in Concrete*, Rock and Ceramics, E. & FN, London.

Wasantha, P.L.P., Ranjith, P.G. and Shao, S.S. (2014b), "Energy monitoring and analysis during deformation of bedded sandstone: Use of acoustic emission", *Ultras.*, **54**(1), 217-226.

Wong, R.H.C. and Chau, K.T. (1998), "Crack coalescence in a rock-like material containing two cracks", *J. Rock Mech. Min. Sci.*, **35**(2), 147-164.

Wong, R.H.C., Chau, K.T., Tang, C.A. and Lin, P. (2001), "Analysis of crack coalescence in rock-like materials containing three flaws-Part I: Experimental approach", *J. Rock Mech. Min. Sci.*, **38**(7), 909-924.

Xie, Z., Peng, F. and Zhao, T. (2014), "Experimental study on fatigue crack propagation of fiber metal laminates", *Steel Compos. Struct.*, **17**(2), 145-157.

Yang, S.Q., Dai, Y.H., Han, L.J. and Jin, Z.Q. (2009), "Experimental study on mechanical behavior of brittle marble samples containing different flaws under uniaxial compression", *Eng. Fract. Mech.*, **76**(12), 1833-1845.

Yang, S.Q., Jiang, Y.Z., Xu, W.Y. and Chen, X.Q. (2008), "Experimental investigation on strength and failure behavior of pre-cracked marble under conventional triaxial compression", *J. Sol. Struct.*, **45**(17), 4796-4819.

Zhang, H.Q., Zhao, Z.Y., Tang, C.A. and Song, L. (2006), "Numerical study of shear behavior of intermittent rock joints with different geometrical parameters", *J. Rock Mech. Min. Sci.*,

43(5), 802-816.

Zhang, X.P. and Wong, L.N.Y. (2012), "Cracking process in rock-like material containing a single flaw under uniaxial compression: A numerical study based on parallel bonded-particle model approach", *Rock Mech. Rock Eng.*, **45**(5), 711-737.

Zhang, X.P. and Wong, R.H.C. (2013), "Crack initiation, propagation and coalescence in rock-like material containing two flaws: A numerical study based on bonded-particle model approach", *Rock Mech. Rock Eng.*, **46**(5), 1001-1021.

Zhao, Y.H., Liang, H.H., Huang, J.F., Geng, J.D. and Wang, R. (1995), "Development of subcracks between en echelon fractures in rock plates", *Pure Appl. Geophys.*, **145**, 759-773.

CC